

**SYNTHESIS AND CHARACTERISATION OF
ZINC OXIDE NANOSTRUCTURES**

SHAHROM BIN MAHMUD

UNIVERSITI SAINS MALAYSIA

2008

**SYNTHESIS AND CHARACTERISATION OF
ZINC OXIDE NANOSTRUCTURES**

by

SHAHROM BIN MAHMUD

**Thesis submitted in fulfillment of the requirements
for the degree of
Doctor of Philosophy**

November 2008

ACKNOWLEDGEMENT

All praises be to the Almighty, Almerciful and Alknowing for permitting me to complete my Phd in Nano-Physics. My deepest gratitude to the following individuals who have provided unparalleled contributions; Prof. Dr. Mat Johar Abdullah and Prof. Dr. Ghanim Putrus for Phd supervision and monetary/research support, Zamzam Zakaria for factory experiments, Dr. Zahid Rizwan for photothermal tests, Muthu for TEM-SAED, Jamilah and Johari for FESEM-EDS, Karuna for XRD, and Djuhaily and Piai for factory electrical testing. Special thanks to my heavenly mother Hajjah Zainiah Abd Hamid for her love and everlasting prayers, and my beautiful wife Dr Hamidah Omar for putting up with my research obsession. And for my pride and joy, my children, who have made it all worthwhile - Haris, Hafiza, Hanim, Hasanah, Husna.

I am indeed indebted to Mr. John Chong and Hj. A. Karim Mohamad, the owners of Approfit ZnO Mfg. Sdn. Bhd. (223363-P), for allowing me to synthesize ZnO nanocrystals using their factory furnaces. And for Prof. Dr. M.A. Alim (Alabama A&M University USA) and Prof. Dr. Ghanim Putrus (Northumbria University UK) - I appreciate your valuable technical advice for the past couple of years. I am honoured by the following persons; Prof. Dr. Prashant Kumta and Prof. Dr. Richard Puddephatt for appointing me as a *journal reviewer* for their Journal of Material Science and Engineering B (impact factor 1.3) and Inorganic Chimica Acta (impact factor 1.7) respectively; WIF organisers for honouring me as a *plenary speaker* for the United Nation's World Innovation Forum 2007 (Kuala Lumpur), and Dr. Peter Robinson for appointing me as an *international consultant* for his Canadian ZnO firm, Integrated Resource Management (131662900 RT0001).

Finally, I express appreciation to everyone, not mentioned here, who had chipped in fragments of assistance to the completion of my Phd work.

TABLES OF CONTENTS

| | Page |
|--|-------------|
| Acknowledgement | ii |
| Tables of Contents | iii |
| List of Tables | vi |
| List of Figures | vii |
| List of Plates | xii |
| List of Abbreviations | xiii |
| List of Symbols | xiv |
| Abstrak | xv |
| Abstract | xvi |
| CHAPTER 1 – INTRODUCTION | |
| 1.1 Nanotechnology Overview | 1 |
| 1.2 Nanotechnology Definition | 3 |
| 1.3 Nanoscale Effects | 3 |
| 1.4 Zinc Oxide Nanomaterials: Current and Future | 4 |
| 1.5 Objectives of Study | 6 |
| 1.6 Scope of Study | 8 |
| 1.7 Background of Study | 10 |
| 1.8 Overview of Thesis | 11 |
| CHAPTER 2 – LITERATURE SURVEY | |
| 2.1 Applications of Zinc Oxide | 15 |
| 2.2 Properties of Wurtzite Zinc Oxide | 17 |
| 2.3 ZnO Crystal Structure and Band Structure | 19 |
| 2.4 Miller-Bravais Wurtzite Structure | 24 |

| | | |
|--|---|----|
| 2.5 | Crystal Growth: Thermodynamic, Kinetics and Facets | 30 |
| 2.6 | Mechanical Properties | 37 |
| 2.7 | Thermal Properties | 40 |
| 2.8 | Electrical Properties | 41 |
| 2.9 | Optical Properties and Defects | 42 |
| 2.10 | Synthesis of ZnO Nanoparticles | 47 |
| | 2.10.1 American and French Processes | 48 |
| | 2.10.2 Flame-Aerosol Synthesis | 54 |
| | 2.10.3 Physical Vapor Synthesis | 56 |
| CHAPTER 3 – EXPERIMENTAL PROCEDURES | | |
| 3.1 | Nanofabrication | 59 |
| | 3.1.1 Catalyst-Free Combust-Oxidized (CFCO) Process | 59 |
| | 3.1.2 Catalyst-Free Combust-Oxidized Rig (CFCOR) Process | 60 |
| | 3.1.3 Catalyst-Free Combust-Oxidized Mesh (CFCOM) Process: Novel Fabrication | 62 |
| 3.2 | Semiconductor Device Preparation | 64 |
| | 3.2.1 ZnO Pelletization for Photoresponse | 64 |
| 3.3 | Characterization | 65 |
| | 3.3.1 Spectroscopy | 65 |
| | 3.3.2 Microscopy | 69 |
| CHAPTER 4 – EXPERIMENTAL RESULTS | | |
| 4.1 | Synthesis and Morphology | 74 |
| 4.2 | EDX Data | 82 |
| 4.3 | XRD Data | 87 |
| 4.4 | Specific Surface Area | 92 |
| 4.5 | Photopyroelectricity and Band Gap | 93 |

| | | |
|---|--|-----|
| 4.6 | Photoluminescence | 95 |
| 4.7 | Photoresponse | 100 |
| 4.8 | Reliability and Confidence Level of Experiment | 106 |
| CHAPTER 5 – ANALYSES AND DISCOVERIES | | 108 |
| 5.1 | Morphology | 110 |
| 5.1.1 | Nanoscopic Inhomogeneity | 110 |
| 5.1.2 | Novel Nanostructures of ZnO | 113 |
| 5.1.2.1 | Novel ZnO Nanoboxes | 114 |
| 5.1.2.2 | Novel ZnO Nanomallets | 121 |
| 5.1.2.3 | Novel ZnO Nanotripods | 134 |
| 5.1.3 | Other Nanostructures of ZnO | 145 |
| 5.1.4 | Tapered Head Simulation of ZnO Nanorods | 153 |
| 5.2 | Novel Nanofabrication | 157 |
| 5.3 | Novel Nano Equation for ZnO Nanorods and Nanowires | 170 |
| 5.4 | Nanostructural-Optoelectronic Correlations | 174 |
| 5.4.1 | General Correlations | 174 |
| 5.4.2 | Insulating Grain Boundaries | 175 |
| 5.4.3 | Probable Origins for Optoelectronic Responses | 184 |
| CHAPTER 6 – CONCLUSIONS | | 192 |
| REFERENCES | | 194 |
| APPENDIX A | RESEARCH PAPER PUBLICATIONS AND CONFERENCES | 206 |
| APPENDIX B | LIST OF PAPERS | 209 |
| APPENDIX C | BET DATA | 224 |

LIST OF TABLES

| | | Page |
|-----------|--|-------------|
| Table 2.1 | Properties of ZnO | 18 |
| Table 4.1 | Synthesis parameters of ZnO samples | 74 |
| Table 4.2 | Morphology Diversity of ZnO Specimens | 75 |
| Table 4.3 | Summary of EDX data on ZnO samples | 82 |
| Table 4.4 | XRD data on normalized intensities (%) of ZnO crystal indices | 88 |
| Table 4.5 | Specific surface area data summary | 92 |
| Table 4.6 | Photoluminescence data | 96 |
| Table 4.7 | Photoluminescence and Band-gap Energy data | 96 |
| Table 4.8 | Steady-state Photoresponse Data | 101 |
| Table 4.9 | Summary of quantum efficiency results for colored light exposure | 101 |
| Table 5.1 | Summary of Experimental Results | 109 |
| Table 5.2 | Description of zones in morphology chart | 165 |

LIST OF FIGURES

| | | Page |
|-------------|--|------|
| Figure 1.1 | Future applications of nano ZnO in the automotive industry | 6 |
| Figure 2.1 | ZnO unit cell with ionic positions of zinc and oxygen atoms. | 20 |
| Figure 2.2 | Zinc interstitial sites in the ZnO wurtzite lattice. | 22 |
| Figure 2.3 | Energy band structure of ZnO. | 24 |
| Figure 2.4 | Four reciprocal lattice vectors of the 4D Miller-Bravais index system | 26 |
| Figure 2.5 | Hexagonal right-prism of ZnO wurtzite structure | 28 |
| Figure 2.6 | Hexagon observed looking down from vertical \mathbf{a}_4^* vector | 28 |
| Figure 2.7 | 4-D simulation of (0001) and $(10\bar{1}0)$ surface planes | 29 |
| Figure 2.8 | 4-D simulation of $(10\bar{1}2)$ and $(\bar{1}011)$ surface planes. | 29 |
| Figure 2.9 | Interfacial tensions of heterogenous nucleation. | 33 |
| Figure 2.10 | ZnO hexagonal crystal indices of basal and side facets | 34 |
| Figure 2.11 | ZnO hexagonal crystal lattice simulation for polar (a) (0001) stacking, and (b) $(000\bar{1})$ stacking | 35 |
| Figure 2.12 | ZnO hexagonal crystal lattice simulation for nonpolar (a) $(10\bar{1}0)$ stacking, and (b) $(11\bar{2}0)$ stacking | 36 |
| Figure 2.13 | Resonance test on one ZnO belt showing TEM images for (a) stationary condition, (b) first harmonic resonance in x-direction, and (c) first harmonic resonance in y-direction | 38 |
| Figure 2.14 | Calculated defect formation energy as a function of Fermi level for main ZnO native defects in zinc-rich and oxygen-rich conditions | 39 |
| Figure 2.15 | Calculated defect formation energy as a function of Fermi level for main ZnO native defects in zinc-rich and oxygen-rich conditions | 45 |
| Figure 2.16 | Schematic diagram of French-process ZnO furnace | 50 |
| Figure 2.17 | Industrial French-process ZnO showing (a) FESEM image with 200nm scale bar, and (b) TEM image with 500nm scale bar | 53 |
| Figure 2.18 | A flame reactor schematic for flame spray pyrolysis | 55 |

| | | |
|-------------|--|----|
| Figure 2.19 | From left, a flame in FSP process, explanatory process schematic and TEM image of flame-synthesized ZnO | 56 |
| Figure 2.20 | (a) PVS technology schematic, and (b) TEM image of PVS-ZnO | 57 |
| Figure 3.1 | Schematic of air rig for CFCOR process | 61 |
| Figure 3.2 | Schematic of French process with steel mesh sieve just above furnace orifice. The location of the sieve mesh is shown with respect to the actual furnace photo. | 62 |
| Figure 3.3 | Transmission spectra of colored plastic films showing peak locations | 67 |
| Figure 3.4 | Schematic of testing set-up for photoresponse I-V measurement | 68 |
| Figure 4.1 | FESEM micrograph showing ZnO particle being captured on TEM grid. | 73 |
| Figure 4.2 | FESEM micrograph of Type 1 morphology with (a) many plate-like structures, and (b) rectangular plates and large polygon plates. | 76 |
| Figure 4.3 | Type 2 morphology with rod-like structures shown in (a) FESEM micrograph, and (b) TEM micrograph | 77 |
| Figure 4.4 | : FESEM micrograph of Type 3 morphology with wire-like structures | 78 |
| Figure 4.5 | FESEM micrograph of Type 4 morphology with multipod structures | 78 |
| Figure 4.6 | FESEM micrograph of Type 5 morphology showing particles with irregular shapes | 79 |
| Figure 4.7 | FESEM micrographs showing nanoscopic inhomogeneity | 79 |
| Figure 4.8 | (a) TEM micrograph showing a quasi-hexagonal drum (CFCO powder), and (b) SAED diffraction pattern of a central spot on the hexagonal drum in (a) illustrating polycrystalline nature with clear diffraction rings | 80 |
| Figure 4.9 | TEM micrograph ZnO nanorods (CFCOR powder) with one of them having a tapered head, and (b) SAED diffraction pattern of a spot, shown by the arrow symbol, on the tapered nanorod in (a) illustrating single crystalline nature | 81 |
| Figure 4.10 | EDX data on ZnO sample | 83 |
| Figure 4.11 | XRD spectra of ZnO sample | 89 |

| | | |
|-------------|---|-----|
| Figure 4.12 | PPE plots for (a) full range, and (b) onset region showing extrapolation | 94 |
| Figure 4.13 | PL spectra of samples | 97 |
| Figure 4.14 | Dark I-V spectra for ZnO pellets | 103 |
| Figure 4.15 | Photoresponse I-V spectra | 104 |
| Figure 5.1 | Multiple ZnO structures co-exist in a minute region | 111 |
| Figure 5.2 | FESEM micrographs showing (a) ZnO nanoplates, and (b) a ZnO nanoplate “resting” on the sidewall of a tapered rod. | 115 |
| Figure 5.3 | FESEM micrographs showing (a) a ZnO nanobox “resting” on the sidewall of a rod, and (b) a ZnO nanobox “slantingly resting” on the sidewall of a rod | 116 |
| Figure 5.4 | TEM micrograph showing two long and “slanted” nanoplates seemingly grown from the side-facets of a nanorod | 117 |
| Figure 5.5 | TEM micrograph showing SAED done on one ZnO nanoplate at a location indicated by the arrow. Diffraction ring patterns are indexed as shown. | 117 |
| Figure 5.6 | Miller-Bravais 4-D simulation for ZnO nanoplate and nanobox | 119 |
| Figure 5.7 | Simulation for nucleation plane | 119 |
| Figure 5.8 | Width (W) and height (H) of nanoplate and nanobox | 121 |
| Figure 5.9 | FESEM micrographs of (a) ZnO nanomallet with bulging prismatic head, small tapered neck and short handle | 122 |
| Figure 5.10 | Longer ZnO nanomallets with rectangular-like head, tapered neck and long handle as seen in (a) FESEM micrograph, and (b) TEM micrograph | 123 |
| Figure 5.11 | TEM-SAED microscopy on one ZnO mallet. | 124 |
| Figure 5.12 | Crystal model for ZnO nanomallets showing (a) head-handle type, and (b) head-neck-handle type | 125 |
| Figure 5.13 | Proposed growth model for ZnO nanomallets | 127 |
| Figure 5.14 | FESEM micrographs of a ZnO nanomallet seemingly grown from one of the $\{10\bar{1}0\}$ side-facets as shown in (a), and the same micrograph with arrows indicating probable growth directions as illustrated in (b) | 131 |
| Figure 5.15 | Proposed growth model for ZnO rectangular nanomallets with oriented growth along $\langle 10\bar{1}0 \rangle$. | 132 |
| Figure 5.16 | Proposed growth model for ZnO rectangular nanomallets with growth direction along $\pm[10\bar{1}0]$ | 133 |

| | | |
|-------------|--|-----|
| Figure 5.17 | ZnO mallet with two handles. | 133 |
| Figure 5.18 | TEM micrograph of one planar nanotripod of ZnO, base-arm type | 134 |
| Figure 5.19 | TEM micrograph showing (a) one base-arm-type nanotripod, and (b) hexagonal patch at the core | 135 |
| Figure 5.20 | FESEM micrograph of (a) ZnO tripod of core type, and (b) the same tripod with dashed lines emphasizing faint lines at the core. | 136 |
| Figure 5.21 | TEM-SAED data from one of the base arm of one ZnO nanotripod | 137 |
| Figure 5.22 | 4-D simulation for ZnO tripods for (a) base-arm type, and (b) core type | 138 |
| Figure 5.23 | Proposed growth mechanism for base-arm ZnO tripods illustrating (a) base arm growth, followed by (b) tapering and more arm growth, and (c) final forms | 140 |
| Figure 5.24 | Proposed growth mechanism for core-type ZnO tripods illustrating (a) core formation, (b) growth of arms, (c) core transformation, and (d) final form | 144 |
| Figure 5.25 | FESEM micrographs showing hexagonal ZnO rods from CFCOR powder. The scale bar is 100 nm. | 146 |
| Figure 5.26 | FESEM micrograph of ZnO whisker consisting nanowires from NORM-10 powder. | 146 |
| Figure 5.27 | TEM micrograph of very long ZnO nanowires from LOW-10 powder. | 147 |
| Figure 5.28 | FESEM micrographs of a ZnO nanotetrapod from NORM-10 powder | 148 |
| Figure 5.29 | FESEM micrographs showing (a) a ZnO tetrapod from NORM-20 powder, and (b) ZnO layers on the erect arm of the tetrapod. | 149 |
| Figure 5.30 | TEM micrographs showing threading dislocations of (a) a ZnO nanorod, and (b) a ZnO nanorod with a long nanoplate | 151 |
| Figure 5.31 | FESEM micrographs of unique nanostructures of (a) ZnO nanorockets, and (b) a ZnO nanokancil | 152 |
| Figure 5.32 | Tapered head facets of (a) one ZnO rod, and (b) a cluster of ZnO nanorods | 154 |
| Figure 5.33 | Tapered head simulations of ZnO rods | 156 |

| | | |
|-------------|--|-----|
| Figure 5.34 | Schematic diagram of CFCOM process. | 158 |
| Figure 5.35 | Model for structural transformation in CFCOM process | 160 |
| Figure 5.36 | (a) TEM micrograph of a long rectangular structure with tapered tip, and (b) FESEM micrograph of a long nanomallet reproduced from Figure 5.10(a). | 161 |
| Figure 5.37 | FESEM micrograph of long acicular nanostructures. | 162 |
| Figure 5.38 | Acicular structures grown from ZnO clusters | 163 |
| Figure 5.39 | TEM micrograph showing ZnO nanoknives. | 163 |
| Figure 5.40 | Morphology chart of CFCOM process at residence time of 10 s | 165 |
| Figure 5.41 | Measurement of ZnO nanowires and nanorods showing (a) length, (b) width variation problem, and (c) width measurement locations | 171 |
| Figure 5.42 | Graph of aspect ratio versus length of ZnO nanorods and nanowires | 172 |
| Figure 5.43 | Nanostructural-Optoelectronic Correlation (part A) | 177 |
| Figure 5.44 | Nanostructural-Optoelectronic Correlation (part B) | 178 |
| Figure 5.45 | Photoresponse ϵ -ratio data | 179 |
| Figure 5.46 | Quantum Efficiency graphs | 180 |
| Figure 5.47 | Model of insulating grain boundary showing trapped charges | 181 |
| Figure 5.48 | Atomic defect model | 181 |
| Figure 5.49 | Defect energy levels in ZnO | 185 |

LIST OF PLATES

| | | Page |
|-----------|--|-------------|
| Plate 1.1 | Photo taken in front of Approfit ZnO Manufacturing Sdn. Bhd, Seremban, with the author at the forefront | 13 |
| Plate 1.2 | Interior of Approfit ZnO Manufacturing Sdn Bhd factory showing 5 furnaces, some of which are used to synthesize ZnO nanocrystals for this work | 13 |
| Plate 2.1 | Photograph of French-process ZnO furnace (left) and ZnO furnace in operation (right) | 50 |
| Plate 3.1 | Steel mesh sieve (Tyler mesh 20) used in experiment, showing powder sticking to the sieve | 63 |
| Plate 3.2 | Paper cups used to make ZnO pellets | 64 |
| Plate 3.3 | Electrode-pin probes on ZnO pellet surface, for I-V measurement | 68 |
| Plate 3.4 | Field emission scanning electron microscope | 71 |
| Plate 3.5 | Transmission electron microscope | 71 |
| Plate 4.1 | Photos of ZnO specimens for (a) CFCOR powder, and (b) NORM-10 powder | 72 |

LIST OF ABBREVIATIONS

| | |
|------------|--|
| ZnO | zinc oxide |
| Nano ZnO | zinc oxide material with at least one dimension less than 100 nm |
| Micron ZnO | zinc oxide material with dimensions exceeding 100 nm |
| XRD | X-ray diffraction |
| FESEM | field-emission scanning electron microscope |
| EDX | Energy dispersive X-ray |
| TEM | transmission electron microscopy |
| SAED | selected area electron diffraction |
| PL | photoluminescence |
| PPE | photopyroelectricity |
| PR | photoresponse |
| I-V | current-voltage |
| MT | metric ton |
| UV | ultraviolet |
| Q1D | quasi-one-dimensional |
| QE | Quantum efficiency |
| CBM | Conduction band minimum |
| VBM | Valence band maximum |
| DSB | Double Schottky Barrier |
| VLS | vapor-liquid-solid |
| VS | vapor-solid |
| SSA | specific surface area |
| BET | Brunauer-Emmett-Teller, represents specific surface area |
| T-pod | tripod and tetrapod |
| RTH | rectangular-to-hexagonal transformation |
| AR | aspect ratio |
| IGB | Insulating grain boundary |
| DAP | Donor-acceptor pair |
| PHS | perturbed-host-state |

LIST OF SYMBOLS

| | |
|--------------------|---|
| G | Gibbs free enthalpy |
| ΔG | change in Gibbs free enthalpy |
| ΔG_V | free energy change per unit volume |
| ΔG^* | minimum free energy |
| H | enthalpy |
| T | temperature |
| S | system entropy |
| r^* | critical radius |
| γ_{SL}^* | solid-liquid interfacial energy |
| γ_{SL} | solid-liquid interfacial tension |
| γ_{NS} | nucleant-solid interfacial tension |
| γ_{NL} | nucleant-liquid interfacial tension |
| T_m | melting point |
| J | nucleation rate per volume |
| f_O | frequency of atomic addition |
| k_B | Boltzmann constant |
| D_L | liquid diffusivity |
| ΔG^*_{HET} | critical energy needed to form a heterogenous nucleus |
| L_V | latent heat of fusion per volume |
| $f(\theta)$ | particle efficacy |
| λ | optical wavelength |
| q | Electronic charge of magnitude $1.60218 \times 10^{-19} \text{ C}$ |
| c | Speed of light, $2.997925 \times 10^8 \text{ m/s}$ or $2.997925 \times 10^{17} \text{ nm/s}$ |
| E_f | Formation energy of defect |
| d_{BET} | Average agglomerate size |
| E_g | Band-gap energy |
| β | optical absorption coefficient |
| h | Planck's constant ($4.135667 \times 10^{-15} \text{ eV}$. or $6.626069 \times 10^{-34} \text{ J.s}$) |
| ν | frequency of oscillation (s^{-1}) |
| ϵ -ratio | Ratio of colored light resistance to dark resistance |
| ψ | aspect ratio |
| L | length of ZnO nanorod/nanowire |
| δ | slope of the ψ - L graph |
| η_0 | initial growth constant |

SINTESIS DAN PENCIRIAN NANOSTRUKTUR ZINK OKSIDA

ABSTRAK

Penyelidikan ini memberi tumpuan kepada nanostruktur zink oksida (ZnO), sintesis, pencirian, kristalografi dan respon optoelektronik. Serbuk nano ZnO dihasilkan di sebuah kilang ZnO menggunakan relau industri di mana fabrikasi nano yang baru dicipta. Fabrikasi nano tersebut dikenali sebagai proses “*pengoksidaan-pembakaran bebas-katalis (CFCOM)*” iaitu penangkapan zink suboksida pada 940-1500 °C diikuti oleh fasa lindap-kejut udara. Tiga nanostruktur (nanokotak, nanotukul dan nanotripod) berjaya ditemui dan dianalisa. Kaedah Miller-Bravais empat-dimensi digunakan untuk menghasilkan model simulasi kristal untuk nanostruktur baru. Satu persamaan nano baru dihasilkan secara empirikal untuk memperjelaskan penumbuhan kristal nanorod dan nanowayar. Beberapa konsep yang baru diperkenalkan termasuk ketidak-homogen nanoskopik, model segiempat, satah nukleasi and transformasi segiempat-kepada-heksagonal. Korelasi nanostruktur-optoelektronik menunjukkan kerintangan elektrik, fotoluminesen, jurang jalur dan fotorespon adalah sensitif terhadap morfologi dan saiz partikel ZnO. Penurunan partikel saiz didapati boleh menambahkan parameter berikut: keluasan permukaan spesifik (dari 4.8 kepada 10.1 m²/g), nisbah relatif oksigen/zink sinaran-x dispersif tenaga (dari 0.74 kepada 1.47), keamatan fotoluminesen ultra-ungu (dari 0.9x10⁶ kepada 5.0 x10⁶ u.a.) dan peratusan nanorod (dari 15% kepada 55%). Walau bagaimanapun, jurang jalur didapati menurun dari 3.29eV kepada 3.19eV. Kecacatan struktur (vakansi dan interstis) dikesan dari fotoluminesen tampak dalam jalur hijau (513-532nm) dan jalur merah (760-769nm). Perbincangan juga dibuat berkenaan punca-punca yang mungkin menyebabkan fotoluminesen tampak dan fenomena fotorespon.

SYNTHESIS AND CHARACTERISATION OF ZINC OXIDE NANOSTRUCTURES

ABSTRACT

This work focuses on zinc oxide (ZnO) nanostructures with regard to their syntheses, characteristics, crystallography and optoelectronic responses. ZnO nano powder is synthesized in a ZnO factory using industrial furnaces where a novel nanofabrication was developed. The nanofabrication is called catalyst-free combust-oxidized mesh (CFCOM) process that is the capturing of zinc suboxide at 940-1500 °C followed by air-quenching phase. Three new ZnO nanostructures (nanoboxes, nanomallets and nanotripods) are discovered and analysed. Four dimensional Miller-Bravais indexing system is employed to make crystal simulations of ZnO nanostructures. A novel nano-equation is empirically created to describe the growth of nanorods and nanowires. Several new concepts and models are introduced including nanoscopic inhomogeneity, rectangular model, nucleation plane and rectangular-to-hexagonal transformation. Nanostructural-optoelectronic correlations suggest that electrical resistance, photoluminescence, band-gap and photoresponse are found to be sensitive to the ZnO morphology and particle size. A reduction in the particle size tend to increase these parameters: specific surface area (4.8 to 10.1 m²/g), energy dispersive x-ray relative oxygen-to-zinc ratio (from 0.74 to 1.47), ultraviolet photoluminescence intensities (0.9x10⁶ to 5.0 x10⁶ a.u.), and percentage of nanorods (15% to 55%). However, the band-gap is found to fall from 3.29eV to 3.19eV. Structural defects (vacancies and interstitials) are detected from visible photoluminescence in the green (513-532nm) band and red (760-769nm) band. Possible origins for the visible photoluminescence and photoresponse phenomena are also discussed.

CHAPTER 1 – INTRODUCTION

1.1 Nanotechnology Overview

By the year 2014, the market revenue for nanotechnology-related products is expected to reach 2.6 trillion US dollars (USD) [1]. Over USD 10.5 billion was spent on nanotech research in 2005, a 23% increase from previous year [2] whereby about USD 9.5 billion (90%) came from US, Europe and Japan combined. Nanomaterials and nanoparticles are forecasted to dominate future development and market of nanotechnology. From a survey funded by the European Commission (2006) [3], four interesting observations are discovered as follows. Firstly, 74% of enterprises working on nanomaterials are small and medium scale enterprises (SMEs). The second finding is that the most important success factors are superior material properties (78%), quality improvement (47%), cooperation with other companies (37%) and collaboration with research organisations (33%). Thirdly, the most important obstacles for the application of nanomaterials by SMEs are problems with production process technology (41%), high production costs (37%), lack of knowledge transfer from scientific communities to SMEs (33%) and small market volume (18%). Finally, 68% of the 190 respondents spend only 10% of their research investment for external research projects - this data implies that most companies carry out research activities on their own.

Several key conclusions from the above survey are SMEs play a leading role in industrialising nanomaterials, superior materials properties is the major motivation, imperfect manufacturing technology causes high production costs, and poor university-

industry collaboration is noted. As a result, the cost of nanomaterials becomes too high for potential manufacturers to use them in their products. Therefore, most of the industrial nano-research activities focus on making their nano-products cheap enough in order to be competitive.

Recently the Malaysian government has formed an enforcement unit known as *NanoTag Special Task Force* to trace the illegal usage of government-subsidised diesel for fishermen [4] whereby the task force was able to trace over 600 million litres of the subsidised diesel using a nanoparticle technology obtained from the USA. For every 8,000 litres of diesel, an amount of 25 mL nano-chemical marker is added (about 3 ppm). To make detection test on suspected smuggled diesel, another chemical is mixed with a sample of the diesel; and if it turns white or pink, the nano-chemical marker is present in the sample and the smuggler is caught. From this exercise, the government was able to save over RM 400 million from the seizure of the subsidised diesel. This Malaysian experience is among the very few nano-success of the benefits of nanotechnology to the society at large.

However, nanotechnology is still at its infancy when it comes to real application. One of the main reasons is the high cost of nanomaterials, as mentioned earlier, that can be hundreds of US dollars per kg or even thousands of US dollar per kg for specialty nanomaterials [1].

1.2 Nanotechnology Definition

According to the USA National Nanotechnology Initiative [5], nanotechnology is defined as “the understanding and control of matter at dimensions of roughly 1 to 100 nm, where unique phenomena enable novel applications”. Nanoparticles are particles with at least one dimension less than 100 nm [6]. The term nanoparticle is sometimes referred to as nanopowder, nanocrystal or nanocluster. Nanostructures refer to textured materials or systems with at least one dimension on the nanoscale [7]. The global enthusiasm on nanotechnology is inspired by Richard Feynman’s speech in 1959 when he mentioned “*to synthesize nanoscale building blocks with precisely controlled size and composition, and assemble them into larger structures with unique properties and functions*”[8].

1.3 Nanoscale Effects

Two major effects of nanoscale dimensions are quantum confinement and very large surface area [6-12]. Firstly, nanometric dimensions can directly affect the energy band structure leading to changes in the atomic structure; this is a phenomenon known as *quantum confinement*. For semiconducting materials, quantum confinement influences their density of states (donor/trap carrier concentration), total energy and thermodynamic stability thereby affecting their optical, electronic and magnetic properties. ZnO nanoparticles tend to exhibit *quantum size effect* for dimensions below 7 nm whereby a pronounced band gap enlargement and blue-shifting can occur from light absorbance test [13,14]. Secondly, nanometric dimensions dramatically increase the surface area-to-volume ratio. For a 1 nm nanosphere with similar density as ZnO (5.6 g/cm^3), the theoretical surface area would be about $536 \text{ m}^2/\text{g}$ [10], and if the nanosphere contains

internal interfaces (grain boundaries), then the surface area would be much greater such that metastable structures can be stable in nanometer-sized systems. The ultrahigh surface-to-volume ratio, combined with a size comparable to the Debye length, makes nanomaterials highly sensitive to surface chemicals; and their size confinement allows bandgap tunability, larger optical gain and ultrafast operation speed [7,11,12].

1.4 **Zinc Oxide Nanomaterials: Current and Future**

The European Commission has listed ZnO nanopowder as one of the major nanomaterials anticipated to be intensely commercialised in 2006-2014 [3]. Zinc oxide nanomaterials has attracted hefty research fundings due to its highly versatile and promising applications in biotechnology (antibacteria, antifungus, antifouling and biosensors), ultraviolet (UV) applications (catalysis, sunscreen, paint, polymer nanocomposite and rubber) and opto-electronics (light emitting diodes, field effect transistors, field emitters, solar cells, toners, sensors). Other applications include ZnO used in ferrite, varistor, cement, pigment, ceramic flux, animal food, pollutant filter, dental filling, hydrogen fuel and nano-textile [12,15-18].

Figure 1.1 illustrates future applications of nano ZnO in the automotive industry [1-5, 7, 10, 16, 20, 26]. Future cars may have ZnO-embedded car seat that can kill microbes, clean on its own and can retard fire. Windows and windscreens can be coated with ZnO nanocomposite layer that repels water, self-cleans and prevents UV penetration. Nanoparticles of ZnO can be added into engine oil to reduce mechanical friction thereby improving fuel-efficiency. Future generation auto engine may be using hydrogen fuel that employs nanoparticles of zinc and ZnO as the media to store and generate hydrogen gas

from water. Car bumpers made from ZnO composites are stronger and possess better scratch resistance. Vulcanized rubber tyres can last longer if nano ZnO is used as the activator and accelerator. ZnO light emitting diodes (LEDs) are very promising products that may be used for the head light and it is said they are very efficient and use much less power than bulbs. Finally car paints that incorporate nano ZnO in its recipe are more durable, water repellent and anti-static.

Globally the world makes over 1 million tons of ZnO per year [19] whereby less than one percent is nano ZnO. 98% of global ZnO is manufactured using gas phase synthesis, namely the French process and American process [20,21]. The biggest users of ZnO are manufacturers of rubber, followed by smaller applications in paints, coatings, varistors, sunscreens, ferrites, medicated powder, animal food and cements. Currently the mass production of nano ZnO is mainly catered for the sunscreen and cosmetics industries whereby nano ZnO (together with titania) serves as the UV absorber. Most sunscreen lotions that uses inorganic nanoparticles (titania and zinc oxide) as the photocatalysts that protect human skin from dangerous UV rays of sunlight whereby inorganic photocatalysts perform better than organic photocatalysts [22]. Most of the work on nano ZnO are still at the basic research stage [3] and it is expected that by 2015, ZnO nanomaterials will be mass produced in a much larger tonnage for various applications in automotive catalysis, sunscreens, antibacterial products, rubber vulcanization, fungistatics, pigments, nano-textiles, high-performance coatings, water treatment, dental fillings, hydrogen fuel systems, chemical sensors, pollutant filters, toners, and optoelectronics [1-3, 20,23].



Figure 1.1: Future applications of nano ZnO in the automotive industry.

1.5 Objectives of Study

This work focuses on ZnO nanostructures and their properties (physical, optical and electronic). Emphasis is given on the synthesis, crystallography and optoelectronic responses. The uniqueness of this work is that all the nanocrystals are synthesized in a ZnO factory (Aprofit ZnO Manufacturing Sdn Bhd located at Seremban) where 5-ton furnaces are used to synthesize the nanoparticles using a novel nanofabrication developed in this work. To date, very little work is being performed on French process ZnO using industry furnaces and this work represents a frontier research on synthesizing

acicular ZnO nanostructures using French process at a reproducible and rapid rate that lasts several seconds.

Four objectives of the work are as follows. The first objective is to study new synthesis methods on the fabrication of ZnO nanostructures using industrial furnaces. The thermodynamics and kinetics of the novel gas phase synthesis are to be described in detail. Variations in the growth parameters, such as temperature and gas partial pressures, are to be investigated in relation to the morphological changes of the ZnO nanostructures. Moreover, changes in dimensions as the temperature changes are also expected to be observed.

The second objective is to investigate novel nanostructures of ZnO using gas phase synthesis techniques. The novel nanostructures are to be subjected to microscopic and spectroscopic analyses such as X-ray diffraction (XRD), field-emission scanning electron microscope (FESEM), energy dispersive X-ray (EDX), transmission electron microscopy (TEM) and selected area electron diffraction (SAED). Crystallographic modeling is to be performed using four-dimensional (4D) Miller-Bravais indexing system and schematics of proposed crystal representations are to be prepared.

Thirdly, emphasis is to given on the study of *intrinsic defects* that exist in ZnO nanoparticles commonly detected via several tests such as photoluminescence (PL), photopyroelectricity (PPE) and photoresponse (PR) experimentations. Foci are to be given on defect-induced photonic emission in the visible range and also on optical absorption leading to photogenerated charge carriers. For photoresponse study, current-

voltage (I-V) spectra are to be plotted upon exposure to visible lights such as violet, blue, green and red. PPE results can reveal impacts of defects on ZnO band gap.

The fourth and last objective is to establish nanostructural-optoelectronic correlations that correlate synthesis (morphology) with optoelectronic responses. This objective should form correlations for the findings achieved in the first three objectives whereby changes in the optoelectronic responses can be explained by the defects, morphology and synthesis.

1.6 **Scope of Study**

Since the work on ZnO covers a wide area, a reasonable scope of study is made in order set direction for this work. Only results and discoveries related to the scope are to be included in the thesis.

The first scope of work is about crystallography. This research work focuses on new nanostructures of ZnO not discovered or reported by anyone. To describe a new crystal structure, these analyses are made; X-ray diffraction, scanning electron microscopy, transmission electron microscopy, selected area electron diffraction and Miller-Bravais crystallography indexing. A description of the synthesis should be presented along with proposed growth models and final crystal schematics. For the crystal models, each crystal facet is labeled in accordance to data obtained from XRD and TEM-SAED.

The second scope is the focus on undoped ZnO synthesized via French process. The motivation of this phd work is inspired by the fact that 98% of the world's ZnO is manufactured via gas phase synthesis referring to the French process and American process [20,21]. Most of this undoped ZnO has purity exceeding 99.5% whereby for this work, high-purity (>99.9%) Australian-imported zinc ingots are used to synthesize the ZnO variants. Only gas phase synthesis (French process) ZnO and the nano ZnO from the newly-invented nanofabrication are experimented here; whereas synthesis on substrates (thin film) are excluded from this work. Other gas phase industrial technologies are also studied in order to highlight the uniqueness of the new nanofabrication reported in this work.

Thirdly, optoelectronic responses are to be experimented according to the following conditions and limitations. In pure and undoped form, ZnO has a very high resistivity up to GΩ.cm range [24] that prevents Hall effect measurements used to obtain its carrier concentration and mobility. However, its as-grown resistance can be obtained from the I-V measurement at room temperature. Because of equipment limitations, PL tests are limited to room-temperature measurements. For PR tests, I-V measurements are taken when ZnO samples are exposed to different visible-light wavelengths while maintaining light intensity at 3,000 lumens/m² for all PR measurements; no time-dependent photocurrent is measured. Only brief comments are offered for the mechanism of band-gap transition and PL/PR responses since the foci of the work are more toward synthesis and crystallography.

1.7 **Background of Study**

Developed 5 decades ago, the French process technology offers the simplest and cheapest industrial method to mass produce ZnO with purity exceeding 99.5% at an affordable price in the USD 3-4 per kilogram range, making it almost irreplaceable by any other method. Most of the global commercial ZnO exist in the form of 0.2-3 micron agglomerates that are made up of primary nanoparticles or nanocrystallites that are clustered together by atomic or molecular bonding [21]. From the author's interactions with industry engineers working for ZnO factories in and outside Malaysia for the past 3 years, it can be concluded that there is very little research work being published on the primary nanoparticles of the French process ZnO despite the fact that most of the world's one-million-ton-per-year ZnO is manufactured using this technology.

Many ZnO manufacturers are facing numerous customers' complaints regarding fluctuating quality of the ZnO delivered to them despite the fact the ZnO specifications, such as specific surface area (SSA) and purity, are within the customers' requirements. From the author's research findings, different morphologies (rods, plates, boxes, wires, tripods, tetrapods, nodular, irregular) of ZnO primary nanoparticles possess different levels of zinc/oxygen concentrations and also different defect species dominancy. Defects refer to intrinsic types that include oxygen vacancies, zinc vacancies, zinc interstitials, oxygen interstitials and antisites species; these intrinsic defects tend to accumulate on the free surfaces (and internal interfaces) of ZnO particles thereby determine the surface states that are known to be electrically and chemically active [6,26]. These *shape-dependent* impacts on ZnO applications (rubber tyres, varistors, sunscreens, cosmetics, anti-microbes, UV coatings, nanotextiles, photocatalysis and photodetection) are not conclusively known.

Future work is needed to study the shape-dependent effects on ZnO major applications especially rubber products, semiconductors, sunscreens and cosmetics. New knowledge that can relate shape-dependent impacts with real applications would possess high commercial value since ZnO manufacturers can use the new knowledge to offer *morphology-customized ZnO* to their customers. The findings of this work have been shared with ZnO global manufacturers in a popular decade-old ZnO forum at <http://www.finishing.com/123/73.shtml> and <http://uk.geocities.com/shahromx/nano.html> whereby representatives from about twenty ZnO factories have participated in the forum and some have commented on the papers published in this work.

It is the motivation of this work to uncover the unique characteristics of the primary nanoparticles of ZnO manufactured via the French process. The missions of this work are to discover and characterize new morphologies of ZnO primary nanoparticles, to identify defect species that dominate the morphology variants, and to study the corresponding shape-dependent impact on the optical and electronic properties of semiconductors.

1.8 **Overview of Thesis**

Literature review on recent ZnO research is presented in chapter 2 that include ZnO properties (crystallography, mechanical, thermal, electrical and optical), nanoparticle synthesis, Miller-Bravais crystallography and intrinsic defects. Emphasis is given on gas phase synthesis for nanoparticle production especially syntheses that possess commercial value. An important tool for nano-research is the simulation of novel nanostructures whereby data obtained from microscopy and spectroscopy is extracted and translated into 4-D Miller-Bravais crystal simulation. Intrinsic defects are the foci of many published papers in which these deep/shallow level defects have a big impact on

optical and electronic responses, and many workers have demonstrated the correlation between these defects and the fabrication parameters.

Chapter 3 deals with experimental procedures employed in this work. All the ZnO nanocrystals in this work are synthesized in a factory, Aprofit ZnO Manufacturing Sdn. Bhd, that is shown in Plate 1.1 . Plate 1.2 shows the factory interior housing several industrial ZnO furnaces that are used to synthesize the nanocrystals. Growth parameters such as temperature and oxidation level are varied to study their impact on the ZnO morphology, dimension and intrinsic defects. Fresh nanoparticles are collected from the factory and characterized. Characterization techniques for microscopy and spectroscopy are typical methods used in advanced materials physics research. For photoresponse, samples are prepared via a novel nondestructive pelletization of the as-grown ZnO.

Research results are presented in Chapters 4 and 5 that include SEM-TEM micrographs of novel ZnO nanostructures (boxes, mallets and tripods) and corresponding 4-D crystal simulations using Miller-Bravais indexing and XRD data. Other known structures such as nanorods, nanowires and nanotetrapods are also briefly reported. Intrinsic defect analysis is done using posted data from PL, PPE, PR and I-V measurements. Chapter 5 offers interesting discussions on the newly discovered ZnO nanostructures and their growth parameters whereby a new growth model is proposed for the novel nanofabrication. A new growth equation is also proposed for commonly found ZnO nanorods and nanowires. Impacts of intrinsic defects are discussed in relation to data from PL, PPE, PR and I-V tests. Finally the last chapter 6 concludes all notable research outputs and suggests future projects on ZnO.



Plate 1.1: Photo taken in front of Approit ZnO Manufacturing Sdn. Bhd, Seremban, with the author at the forefront.



Plate 1.2: Interior of Approit ZnO Manufacturing Sdn Bhd factory showing 5 furnaces that are used to synthesize ZnO nanocrystals for this work.

The uniqueness of this work lies in the strong industrial collaboration with the engineers and staff of Aprofit ZnO Manufacturing Sdn Bhd. Since all the ZnO nanocrystals in this work are synthesized using 5-ton industrial furnaces, this work can be classified as industrial nanoparticle research in that the corresponding research outputs would possess great commercial value.

Another interesting fact of this work is the international collaboration with a global ZnO expert from Canada, a ZnO varistor expert from Northumbria University, and also with fellow workers from Universiti Putra Malaysia. Many joint-papers have been published in ISI journals, national journals and international conferences that can validate research outputs from this work.

In a nutshell, the research outputs of this work include four impact-factor journal papers, three national journal papers, eight international proceedings, three citations from ISI Citation Index, discovery of three novel ZnO nanostructures, one nanofabrication and one new nano-equation. Appendix A provides a list of all publications and related conferences while Appendix B lists down front pages of journal papers and selected publications.

CHAPTER 2 – LITERATURE SURVEY

2.1 Applications of Zinc Oxide

Zinc oxide (ZnO) has attracted huge research effort due its potential versatile applications in ultraviolet (UV) photodetectors, chemical sensors, transparent electronics, spintronics, UV light emitters, surface acoustic devices, piezoelectric transducers, mechanical resonators, short-wavelength electronics, field effect transistors, logic gates, optical memory, light emission diodes, photovoltaic devices, superconductors, UV polymer nanocomposites, bacteria DNA detection, neuro networks, hydrogen fuel engine system, engine oil tribology, water treatment and rubber nano-accelerators [1-5, 7-12, 16-27-32]. The photo in Plate 1.1 illustrates future applications of nano ZnO whereby the applications do not merely limit to automobiles but instead extend to other larger areas including future photonics, nanoelectronics, biotechnology, drug delivery, nano coatings and space applications.

The current applications of nano ZnO are very few in that the biggest users of nano ZnO are the sunscreen, cosmetics and pharmaceuticals industries, accounting for over 20000 metric ton (MT) in term of yearly consumption [33]. Normally nano ZnO serves as an additive to sunscreen skin lotion, antiseptic soap/cream, antiseptic plaster, deodorant, anti-rash talc/cream, lipstick and facial cosmetics. The salient properties of nano ZnO that make it suitable for these healthcare products are anti-UVA, anti-UVB, antiseptic, anti-microbial, deodorant, transparency, photo-stability, anti-aging, anti-fungus and anti-rash [33-35]. Eventhough there has been a global concern [22] on skin penetration of ZnO nanoparticles, work done by Cross et al, Gamer et al, Lademann et al, and Nohynek et al,

have proven that nano ZnO (20-30 nm) is safe for human external usage whereby the penetration is very small (1.5-2.3%) and limited to the epidermis (dead skin cells) [33,36-38]. In fact, they found that nano ZnO is much safer than organic-based sunscreen agents that penetrate deeply into the flesh and organic agents are suspected to cause cancer. These recent findings would certainly promote research on nano ZnO since it is now proven that ZnO nanoparticles are biosafe, biocompatible and do not pose a real threat to researchers or workers as long as the powder is not inhaled.

It is also worthy to note one of the earliest applications (in the 1970's) of nano ZnO is its function as the semiconductive-photoconductive agent for photocopy papers. Coloring dyes are absorbed on the large surfaces of ZnO that converts invisible short-wavelength light and long-wavelength infrared into visible light. [39,40]. Recent industrial work on nano ZnO has paved way for initial applications in nano-textiles whereby ZnO nanoparticles are embedded in polymer fabrics in order to introduce intriguing functions especially anti-UV, water repellent, antiseptic, deodorant, self-cleaning, wrinkle-free, fire-retardant, strength enhancing and anti-microbial [30, 41]. These novel textiles seem to produce wonder shirts and wonder jeans; however, the main obstacle still lies in the high cost of nano ZnO that exceeds USD 30/kg that makes nano-textiles too expensive for common public use.

Despite progress in nano ZnO applications, micron-sized ZnO (micron ZnO) is still the dominant type that rules the global versatile applications that include rubber tyres, rubber products, ceramics, varistors, ferrites, paints, coatings, electronic glasses, fungistatic plastic packages, cements, anti-fouling marine coatings, livestock feed additives, cigarette filters, gas/fluid filters, and soil fertilizers [20, 21, 23]. Zinc oxide is used in these products

due to its unique benefits such as anti-UV, anti-aging, strength reinforcement, white-pigmentation, sintering fluxing, anti-microbial, antiseptic, flame retardant, water repellent, self-cleaning, anti-fungus, anti-fouling, anti-algae, HCN-H₂S filtering, animal growth stabilizing, plant growth regulator, ferrimagnetism, semiconducting and high-power energy handling. These highly versatile applications of zinc oxide might explain why zinc is the fourth largest metal being mined in the world after iron, aluminium and copper.

2.2 Properties of Wurtzite Zinc Oxide

The main properties of bulk ZnO [12,26,42-44] is listed in Table 2.1. Kindly note that the data in Table 2.1 refers to bulk ZnO (micron ZnO) whereby the data alters, as ZnO size shrinks down to nanometric level, due to quantum size effects. One commonly found effect of quantum confinement is the increase of the band gap energy especially for quasi-one-dimensional (Q1D) ZnO due to surface state enhancement in response to reduction of nanorods' diameter [6,11,12,26]. Moreover, another impact of Q1D ZnO downsizing is the corresponding carrier concentration change that renders nano ZnO to exhibit novel responses that are not observed when ZnO is in the micron size. These Q1D or rodlike or acicular nanostructures can function as the building blocks for future nanoscale devices, as envisioned by Richard Feynman almost 5 decades ago.

In the next few pages, the literature survey covers ZnO crystal structure, its properties (mechanical, thermal, electrical, optical), defects and growth synthesis.

Table 2.1: Properties of ZnO [12, 26, 42, 44]

| Properties | Value |
|---|---|
| Lattice Constants (at 300K) | a_o 0.32495 nm |
| | c_o 0.52069 nm |
| | c_o / a_o 1.602 (1.633 for ideal case) |
| Density | 5.606 g/cm ³ |
| Molecular weight | 81.39 |
| Stable phase (at 300K) | Wurtzite, $P6_3mc$ space group |
| Melting point | 1975°C |
| Relative dielectric constant | 8.66 |
| Band gap energy | 3.4 eV, direct |
| Intrinsic carrier concentration | $< 10^6$ cm ⁻³ |
| Exciton binding energy | 60 meV |
| Electron effective mass | 0.24 |
| Electron mobility (at 300K) for low n-type conductivity | 200 cm ² /V.s |
| Hole effective mass | 0.59 |
| Hole mobility (at 300K) | 5-50 cm ² /V.s |
| Atomic density | 8.87×10^{22} atoms/cm ³ |
| Ionicity | 61.6% |
| Thermal conductivity | 1-1.2 W/cm.K |
| Thermal electrical conductivity | 0.600 V/cm.K |
| Linear expansion coefficient (at 300K) | $a_o: 6.5 \times 10^{-6}/K$, $c_o: 3.0 \times 10^{-6}/K$ |
| Specific heat (at 300K) | 494 J/kg.K |
| Heat of formation (at 300K) | - 350 kJ/mol |
| Debye temperature | 416K (143°C) |
| Refractive index (555nm wavelength) | a-dir: 2.008, c-dir: 2.029 |
| Modulus of Hardness (MOH) scale | 4 - 5 |

2.3 ZnO Crystal Structure and Band Structure

Zinc oxide is a II-VI compound semiconductor that normally crystallizes in a hexagonal wurtzite (B4) structure in which each anion is surrounded by four cations at the corners of a tetrahedron with a typical sp^3 covalent bonding [11,12,42]. Other crystal structures of ZnO are rocksalt (B1) and zinc-blende (B3) structures. Based on the first principle periodic Hartree-Fock linear combination of atomic orbitals theory by Jaffe and Hess [45,46], the wurtzite is found to be the most thermodynamically stable phase. Jaffe et al also studied the sum of the total energies of isolated neutral zinc and oxygen atoms using the generalized gradient approximation and reported a value of -7.69 eV which is close to the experimental value of -7.52 eV [46].

The ZnO wurtzite unit cell, with a hexagonal close-packed lattice type, has lattice parameters, $a_o = 0.32495$ nm and $c_o = 0.52069$ nm, in the ratio of $c_o / a_o = 1.602$, and it belongs to the space group of $P6_3mc$ [12, 44]. As illustrated in Figure 2.1, the ZnO unit cell consists of four ions (two Zn^{2+} and two O^{2-}) in which the zinc and oxygen ions are tetrahedrally coordinated giving rise to equal positioning to each other [47]. The values of ZnO lattice constants are sensitive to the presence of structural point defects (vacancies and interstitials) and extended defects (threading/planar dislocations) [48] that are commonly found in ZnO resulting in a non-stoichiometric compound $Zn_{1+d}O$ with an excess zinc [49-51]. These excess zinc atoms have the tendency to function as donor interstitials that give its natural n-type conductivity. For nano ZnO, the concentration of zinc/oxygen atoms residing on the surface is greatly enhanced due to the very large surface area, and this affects its density of states rendering it with novel physical, chemical and optoelectronic responses [6, 26].

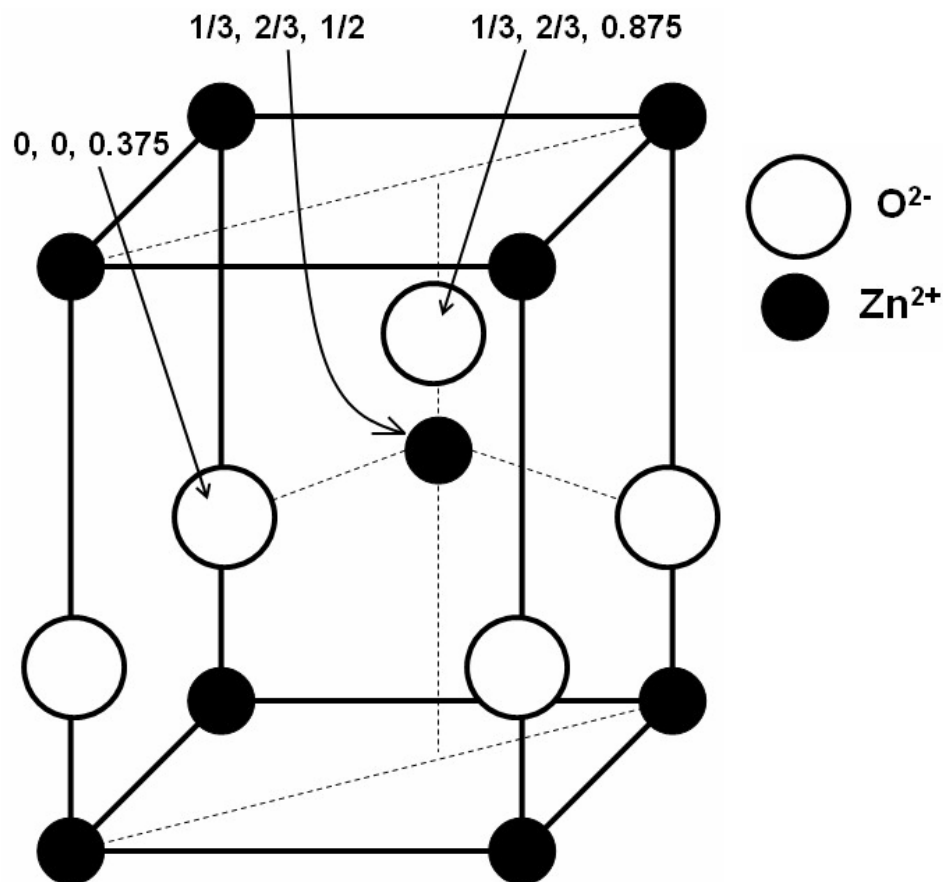


Figure 2.1: ZnO unit cell with ionic positions of zinc and oxygen atoms. Redrawn from [47]

Apart from excess zinc, another unique phenomenon that explains ZnO natural negative conductivity is its strong sensitivity to normal light at room temperature [52]. Once exposed to white light, even at room temperature, ZnO readily deforms by basal (0001) plane slip [52,53]. The deformation may exist in the form of edge or screw dislocations that are caused by the strain on ZnO crystals due to the flow stress developed by the light exposure. Once ZnO is exposed to illumination, each Zn⁺ interstitial ion in the ZnO material is ionized into Zn²⁺ while freeing one electron in the process of ionization. This lonely electron attaches itself to one dangling bond in the dislocation line of either the edge/screw dislocation [47,53-56]. Dangling bonds in the dislocation lines function as

electron trappers that attach free electrons into their dislocation; this phenomenon can explain the ZnO n-type conductivity generated by intrinsic Zn⁺ interstitial donor ions. The ZnO microstructural disorder is commonly found in nano ZnO as indicated by defect-induced photoluminescence in the visible range (violet-blue-green-yellow-red) that is usually attributed to structural defects especially oxygen vacancies, zinc vacancies and zinc interstitials [24,26,42].

In ionic form, the excess zinc exist as Zn⁺ interstitials that are mobile and they tend to occupy special interstitial sites with Miller index ($\frac{1}{3}$, $\frac{2}{3}$, 0.875) as shown in Figure 2.2 [52,54]. These special sites offer passage routes for zinc interstitials to easily migrate within the ZnO wurtzite structure. In the ZnO hexagonal close-packed (HCP) wurtzite structure, there is one octahedral interstitial site per unit cell and 16 tetrahedral interstitial sites per unit cell, giving rise to a maximum of 17 interstitial sites per unit cell [47]. Therefore these 17 interstitial sites, in addition to ($\frac{1}{3}$, $\frac{2}{3}$, 0.875) site, can be occupied by intrinsic zinc interstitials and extrinsic dopant interstitials, provided that the atomic radius ratio is in the range of 0.225-0.732 [47,52]. A common additive for ZnO varistors, bismuth is expected to have difficulty in occupying the interstitial sites due to its large ionic radius (0.12 nm) and it is normally segregated to the grain boundary where it forms bismuth-rich phase that is crucial for the formation of the varistor action (band-bending capability) [57]. Bismuth also contributes in providing oxygen diffusion paths that facilitate the formation of grain boundary electrical states or Schottky potential barriers [49,51].

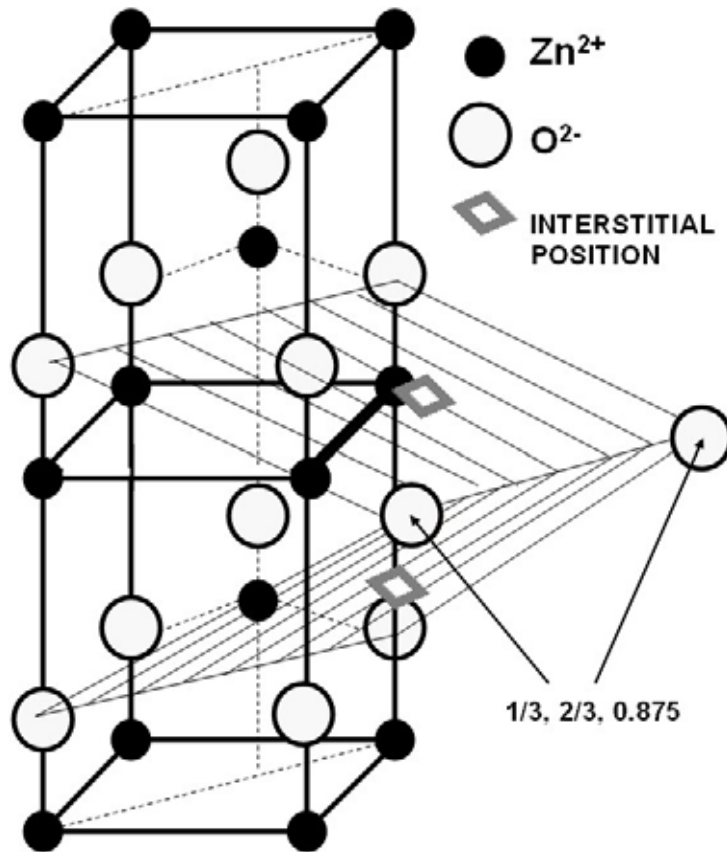


Figure 2.2: Zinc interstitial sites in the ZnO wurtzite lattice. Redrawn from [52,54]

The topic on ZnO defects has been a highly debated one for the past decade since it is difficult to prove the dominant defect species that affect the electron transport in ZnO, the photoconductivity and photoresponse. Based on circumstantial evidence from annealing atmospheric tests and structureless green photoluminescence emission, many workers attributed oxygen vacancies as the most prominent defect species that affect electron transport in micron ZnO and nano ZnO [58-62]. The understanding on the mechanism of defect-controlled electron transport is crucial in fabricating reproducible optoelectronic devices. For the case of ZnO varistor, the double Schottky barrier (DSB) model seems to be accepted by many quarters as the model that offers reasonable mechanistic explanation for the electron transport of the varistor action in the nonlinear current-voltage

region [49,51,63]. However for nano ZnO, there have been many conflicting views regarding the electron transport since most of the views are empirical-based.

Figure 2.3 shows the energy band structure of undoped ZnO. Note that the minimum band gaps range from 3.1 eV to 3.3 eV thereby qualifying pure ZnO to be categorized as an intrinsic semiconductor [49,56,64,65]. With the addition of dopants, the energy band structure will be modified by band bending effects caused by the donor levels. The location of Zn 3*d* level has been determined to be 7.5 eV below the valence band maximum based on UV photoemission measurements by Powell et al. [66,67]. Other similar work reported a value of 8.5 eV [68] and 8.81 eV [69]. Duke et al. studied the ZnO nonpolar ($10\bar{1}0$) surface that is terminated with equal number of O and Zn atoms using low-energy electron-diffraction (LEEDS), and they found that the ($10\bar{1}0$) surface relaxation influences the energies of O 2*p* dangling-bond state and Zn 4*s* dangling-bond state [70]. These two dangling-bond states have been assigned to the Γ , *M* and *X* points of the surface Brillouin zones [71]. Girard et al. reported two binding energy for the (0001) surface, that is 7.5 eV related to the Zn 4*s* – O 2*p* mixed bulk states and 4.5 eV below the Fermi level related to Zn 4*p* – O 2*p* derived states [72]. Local-density approximation studies done by Schroer et al. suggested that the dangling-bond bands are formed within the band gap above the upper edge of the projected bulk bands [73]. Debate on the ZnO band structure has been ongoing among theoretical physicists, and despite many disagreements, some results seem to have good agreement with experimental data thereby offering some light in providing explanation for the defect-induced electron transport in ZnO.

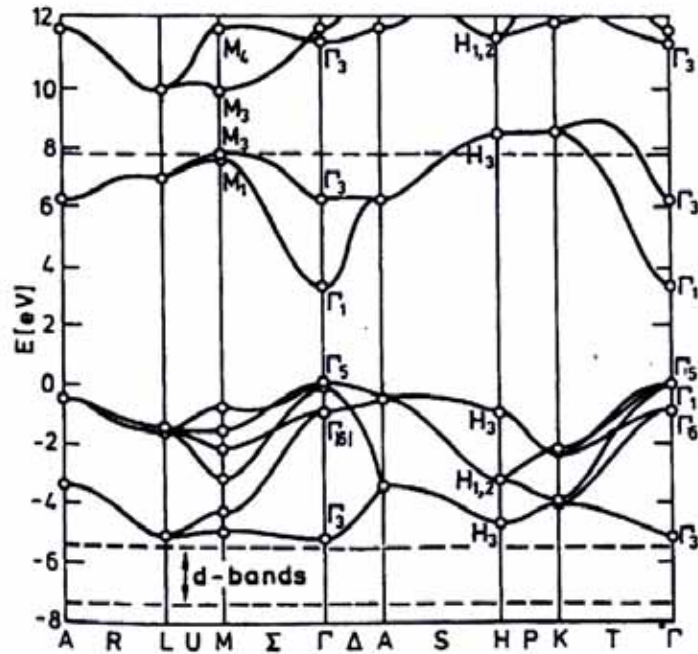


Figure 2.3: Energy band structure of ZnO. Taken from [54,65].

2.4 Miller-Bravais Wurtzite Structure

The 4-dimensional (4D) Miller-Bravais indexing system is a convenient and useful tool in providing crystal simulation of novel ZnO nanostructures [15,74]. Nanostructure modeling is an elemental skill that can offer some light to the possible crystal surfaces that are observed from morphological analyses. From the model, probable growth mechanism can be suggested and investigated. Understanding on the nanostructure morphology can assist us in manipulating fabrication processes in order to achieve selective growth of a desired morphology. In return, unique quantum confinement effects can be maximized from the desired crystallographic orientations that will one day translate into the prototyping of novel nanodevices of immense commercial value. Due to the ZnO diverse morphologies in 1D and 2D systems, there is an obvious need to perform structural